Overview of Disruption-Related Research at UW-Madison

Carl Sovinec, Abdulgader Almagri, Matthew Beidler, Kyle Bunkers, Brett Chapman, Brian Cornille, Ami DuBois, John Goetz, Karsten McCollam, and Stefano Munaretto

University of Wisconsin-Madison

Theory and Simulation of Disruptions Workshop

July 20-22, 2016   Princeton Plasma Physics Lab

Outline

- Introduction
- Computations of vertical displacement and external kink
- Verification of forced magnetic reconnection and mode locking
- Study of runaway-electron generation, suppression, and confinement in MST
- Concluding remarks

Introduction: Research at the Univ. of Wisconsin-Madison contributes to solving the challenges of disruption.

- Computational studies and development for the NIMROD code (https://nimrodteam.org) aim toward characterizing disruptive behavior.
  - Recent efforts focus on numerical improvements.
- Research on runaway electrons (RE) in MST contribute to the ITPA MHD, Disruptions and Control topical group:
  - Generation and suppression of REs in a unique regime
  - Systematic experimental study of confinement with RMPs
  - Simulations of RMP effects on MST tokamaks

Our computations use fluid-based models, visco-resistive MHD in the computations presented here.

- Fluid-based models describe the evolution of low-order moments of particle distributions and low-frequency electromagnetics.

$\frac{\partial n}{\partial t} + \nabla \cdot (n\mathbf{V}) = 0$	particle continuity
$mn\left(\frac{\partial}{\partial t} + \mathbf{V} \cdot \nabla\right)\mathbf{V} = \mathbf{J} \times \mathbf{B} - \nabla(2nT) - \nabla \cdot \underline{\Pi}$	momentum density
$\frac{n}{\gamma - 1}\left(\frac{\partial}{\partial t}T + \mathbf{V} \cdot \nabla T\right) = -nT\nabla \cdot \mathbf{V} - \nabla \cdot \mathbf{q}$	temperature evolution
$\frac{\partial \mathbf{B}}{\partial t} = -\nabla \times (\eta\mathbf{J} - \mathbf{V} \times \mathbf{B})$	Faraday's law & MHD Ohm's
$\mu_0 \mathbf{J} = \nabla \times \mathbf{B}$	Ampere's law
$\nabla \cdot \mathbf{B} = 0$	divergence constraint

- NIMROD is used to solve linear and nonlinear versions of this system.

Computations of VDE and EK: Fundamental aspects of axisymmetric VDE modeling have been established.

- Previous axisymmetric results demonstrate time-scale separation of hot VDE and presheath flows near contact with a resistive wall.

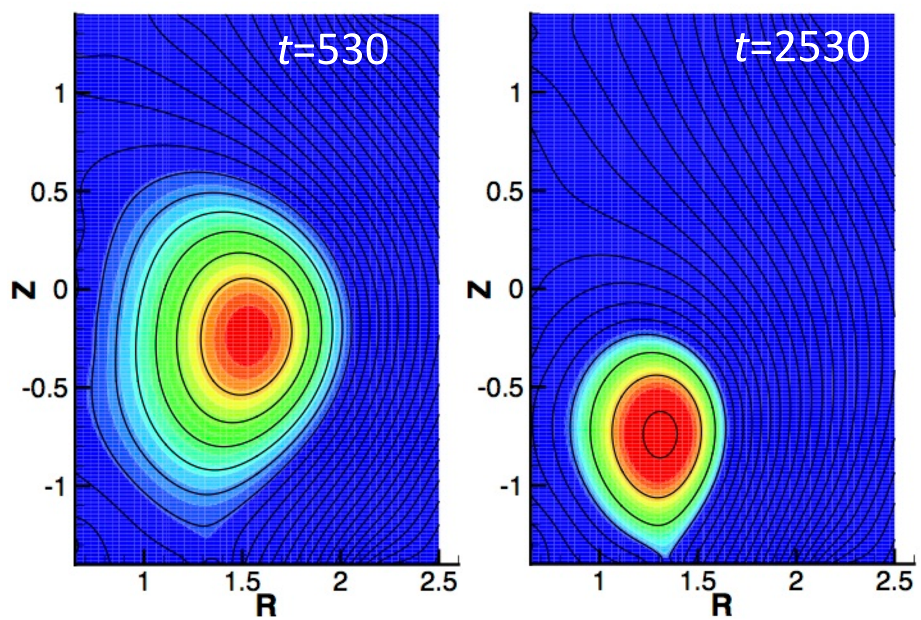

Computed axisymmetric VDE with $\tau_A \ll \tau_w \ll \tau_r$ retains central pressure.

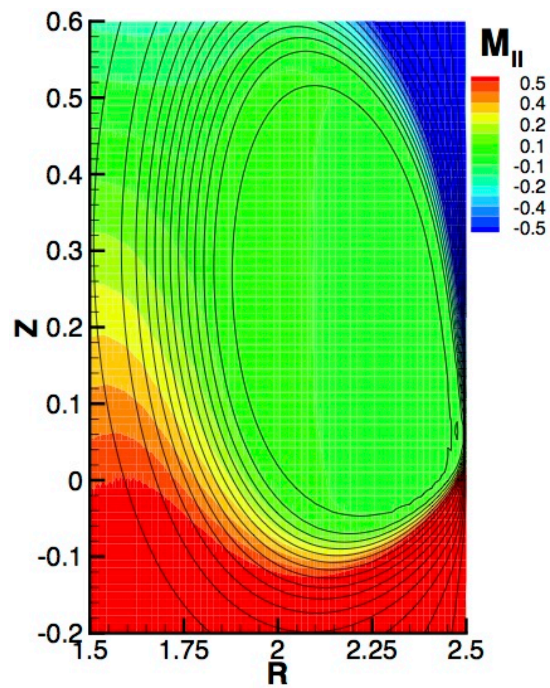

Near-sonic parallel flow develops around confined region; color=$M_{||}$, lines=c_{ia}.

More recent efforts focus on nonlinear external kink dynamics.

- We previously verified linear cylindrical external kink (TSD 2014).
- Nonlinear cylindrical (1,1) kink computations with q_{plasma} = 0.96, L_z/a = 10 reproduce bubble-swallowing of Kadomtsev and Pogutse [Sov. Phys.-JETP 38, 283].

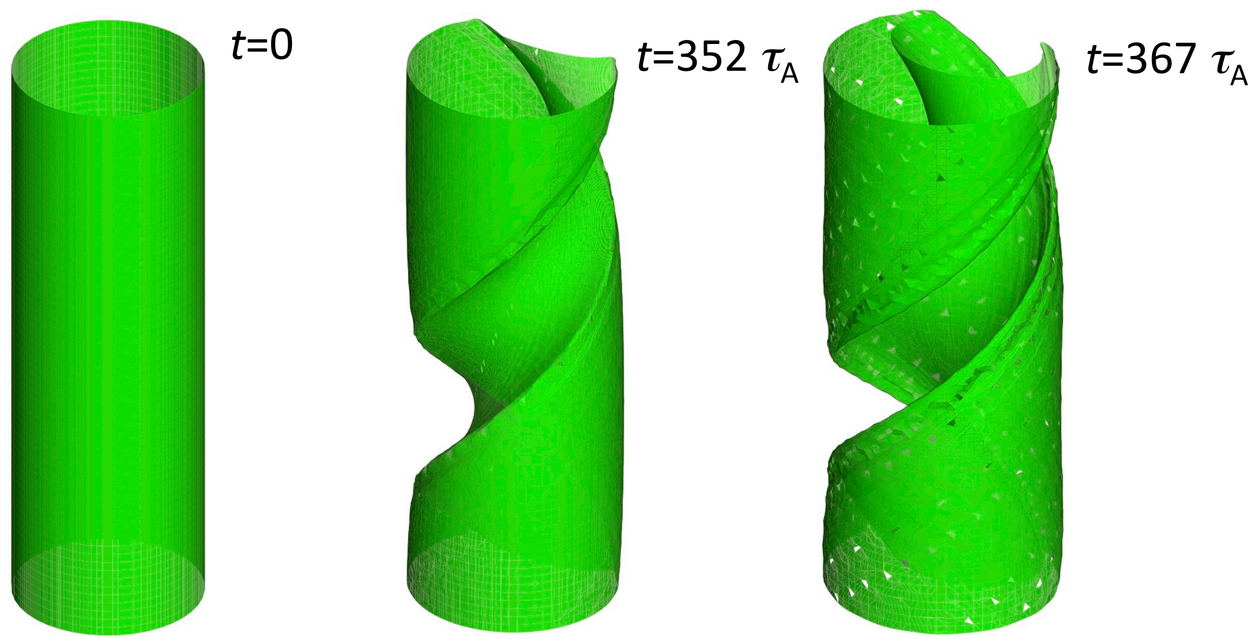

Isosurfaces of density at 0.5 n_{max} illustrate the kink dynamics during the nonlinear evolution.

Nonlinear computations for cylindrical-(2,1) and toroidal kink have also been performed.

- The cylindrical (2,1) problem specification is similar to that of the (1,1) problem, except that $q_{plasma} = 1.9$.
- The toroidal case has $q_{plasma} \cong 0.7$ and multiple harmonics of (1,1) are unstable.

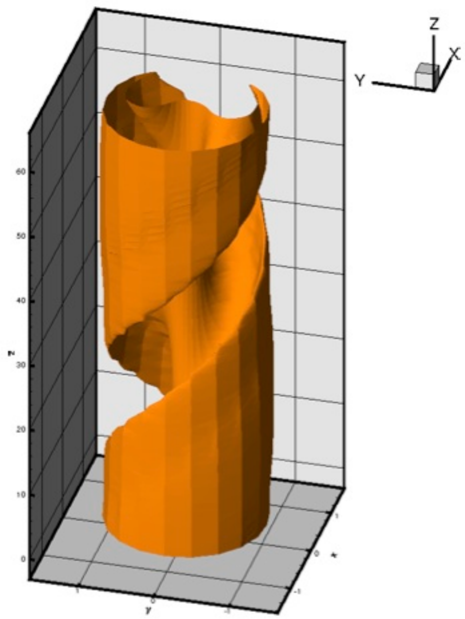

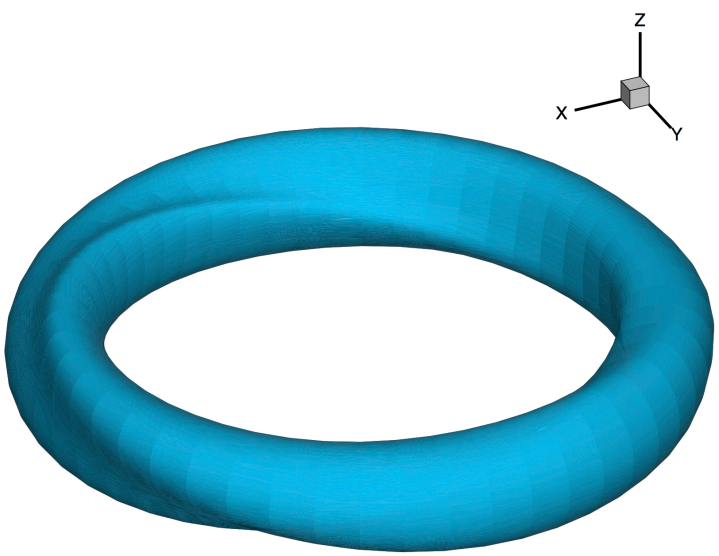

Isosurface of density at 0.1 n_{max} and t = 870 τ_A.

Isosurface of pressure at $p_{max}/8$ and t = 387 τ_A.

Even these relatively small nonlinear calculations pose computational challenges.

- The parameters are modest relative to experimental conditions:
  - S = 3200 ; Pm = 1
  - $T(0) = 1000\ T_{\mathrm{edge}}$; $n(0) = 10\ n_{\mathrm{edge}}$
  - $\eta(T) \sim T^{-3/2}$
- These Eulerian MHD computations distinguish plasma and "vacuum" by $n(\mathbf{x},t)$ and $T(\mathbf{x},t)$ with $\eta(T)$.
  - Large resistivity suppresses current density outside the plasma region.
  - It does not preclude plasma-surface currents.
- Computations need to represent the evolving geometry of the plasma surface.
  - This requires sufficient spatial resolution.
  - Advection of edge profiles is important.
  - Matrices from the implicit **B**-advance with 3D-η are solved at each step.

Limited use of the least-squares finite-element method improves the robustness of NIMROD's advection.

- When advection is stronger than dissipation at the mesh scale, conventional Galerkin projection leads to noisy solutions.
  - Noise in the low-*n* low-*T* regions leads to unphysical negative values.
- LSQFEM uses an alternative projection. [See Bunkers-Sovinec poster for details.]
  - We have applied this to NIMROD's *n* and *T* equations to improve robustness for the kink computations.

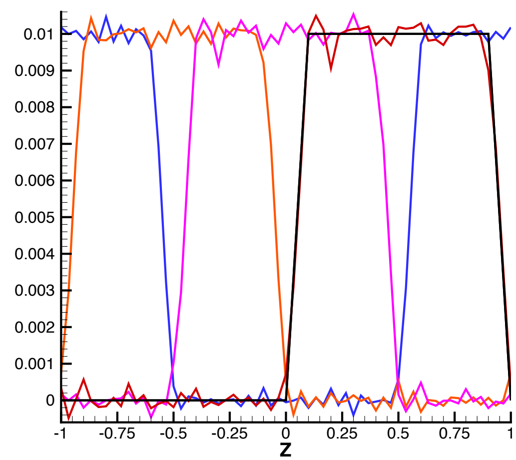

Advection without dissipation produces mesh-scale noise with Galerkin projection.

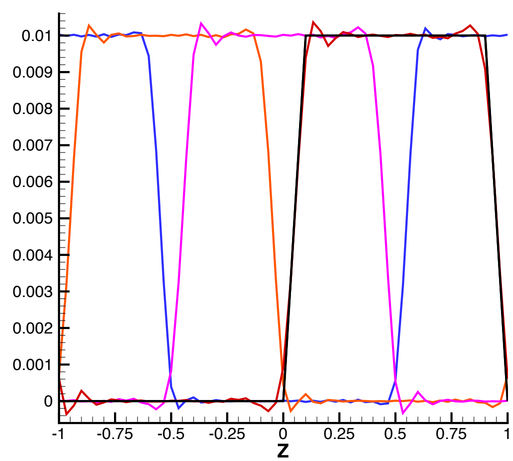

Least-squares projection avoids noise but does not prevent overshoot.

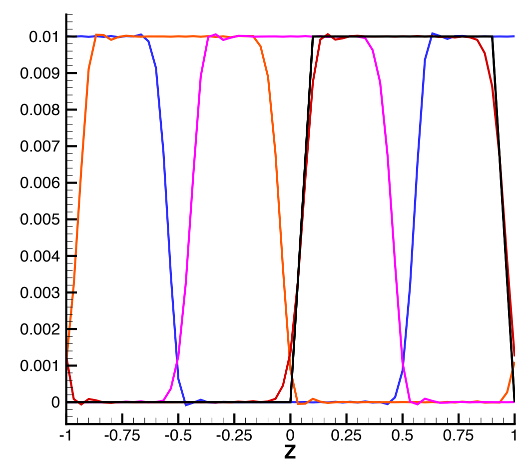

Least-squares projection with limited upwinding reduces overshoot.

The most restrictive aspect of our computations is solving the matrix for the implicit **B**-advance.

- NIMROD uses finite and spectral elements over two coordinates and Fourier series over the third (periodic) coordinate.
  - Matrices are sparse over indices of the meshed coordinates.
  - They are dense with respect to Fourier-component index (n).
  - The magnitude of the Fourier-component coupling depends on the asymmetry of $\eta(\mathbf{x})$.
- We use Krylov-space methods at each timestep to solve algebraic systems.
  - Computational performance depends on preconditioning.
  - Our standard preconditioner applies direct solves to 2D, diagonal-in-n blocks.
  - This looses effectiveness for the **B**-advance when $\eta(\mathbf{x})$ varies strongly over the periodic coordinate.

We have examined a number of methods for improving preconditioning for the **B**-advance.

- Limited Fourier coupling via block-Gauss-Seidel-like relaxation does not help with strongly varying $\eta(\mathbf{x})$.
  - This approach has been used for the Hall term in two-fluid computations.
- Tests for spectral multi-grid show essentially no benefit when using the solution from one level to accelerate the next finer level.
- Direct solves of ϕ-plane based blocks are complementary to the Fourier-based blocks.
  - Applying both at each Krylov step and averaging is somewhat beneficial.
  - Alternating between the two in consecutive steps of flexible-GMRES (FGMRES) reduces the iteration count by 2 to 3.

✧ More information on each method is presented in the Bunkers-Sovinec poster.

Forced reconnection and mode locking: Verification and benchmarking establish a basis for simulating locking during disruptions. [M. Beidler]

- Verification of forced magnetic reconnection in slab geometry uses the analytical results of Hahm and Kulsrud. [PF 28, 2412]
  - The reconnecting component of **B** varies linearly across the domain.
- Edge perturbations drive reconnection.
- Parameters of the computation include:
  - $S = 3.5\times10^5$; $Pm = 1\times10^{-3}$
  - Linear layer width = 5×10^{-3}
  - $B_{\text{guide}} = 100\ B_{\text{rec}}$

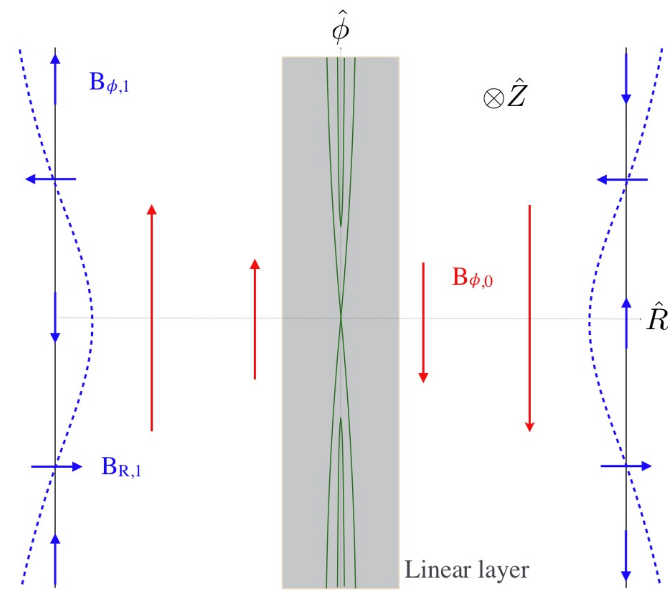

Slab-geometry configuration for forced reconnection.

Linear and nonlinear NIMROD computations reproduce the salient aspects of the HK analysis.

- Linear computations reproduce overshoot of B_{norm} at the resonance.
  - Scaling of preceding growth is nearly $t^{5/4}$.
  - Decay to asymptotic value is somewhat stronger than HK's $t^{-5/4}$.
- Nonlinear computations with $\delta/a > S^{-4/5}$ differ qualitatively from the linear behavior.
  - Computed growth is ~ $t^{0.85}$; HK predict $t^{2/3}$.
  - HK predict that overshoot of B_{norm} is lost for $\delta/a > S^{-4/5}$, and the computations reproduce this effect.
  - Nonlinearly driven harmonics are non-negligible.

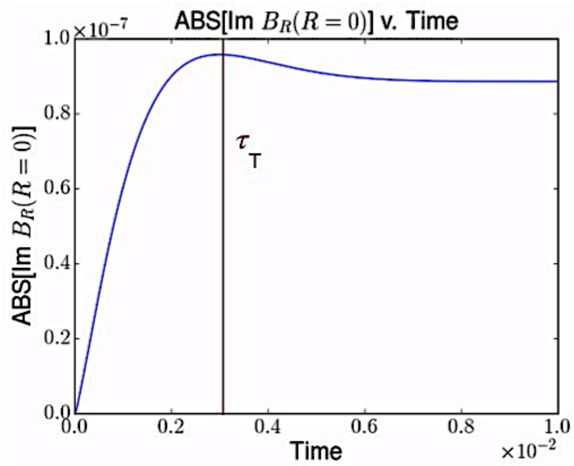

Linear evolution of $B_{norm}(0)$.

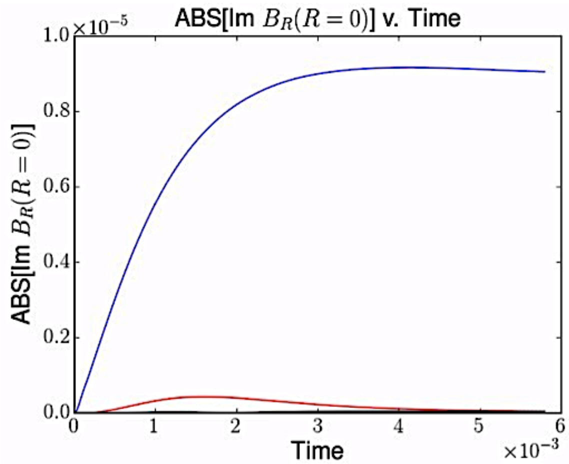

Nonlinear evolution of $B_{norm}(0)$ with $\delta/a \cong 10\ S^{-4/5}$.

Slab-geometry verification of the effects of flow is based on Fitzpatrick's analysis.

- Computations in slab geometry* have been compared with Fitzpatrick, PoP 5, 3325.
  - The analysis elucidates dependences on viscosity, flow, and resistivity (four regimes).
  - With sufficient flow, Alfvén-resonances affect the structure of the solution.
- NIMROD linear computations reproduce:
  - Scaling with V_0 and
  - Alfvén resonances

*Benchmarking with M3D-C1 in cylindrical geometry is underway.

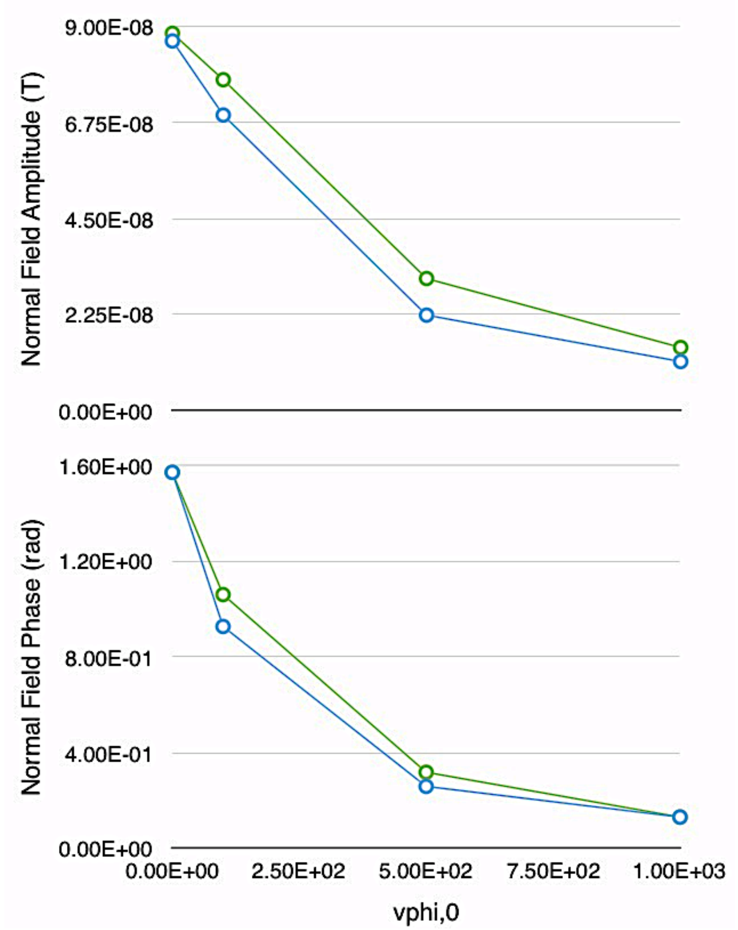

Analytical (blue) and computed (green) scaling of linear B_{norm} amplitude (top) and phase (bottom) in VR regime.

Nonlinear computations reproduce bifurcation above Fitzpatrick's critical flow speed.

- Two saturated states are possible above a critical imposed-flow speed.
- NIMROD simulations reproduce the bifurcation.

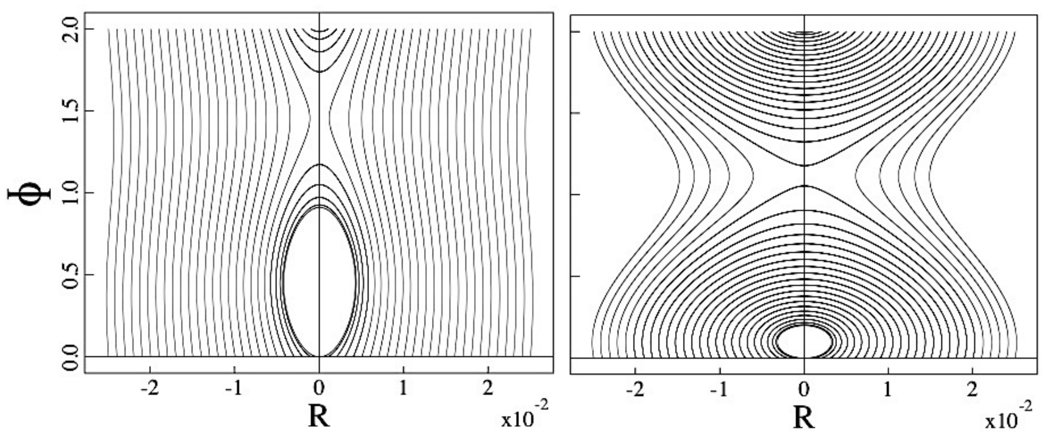

Computed magnetic islands for the high-flow (left) and low-flow (right) states.

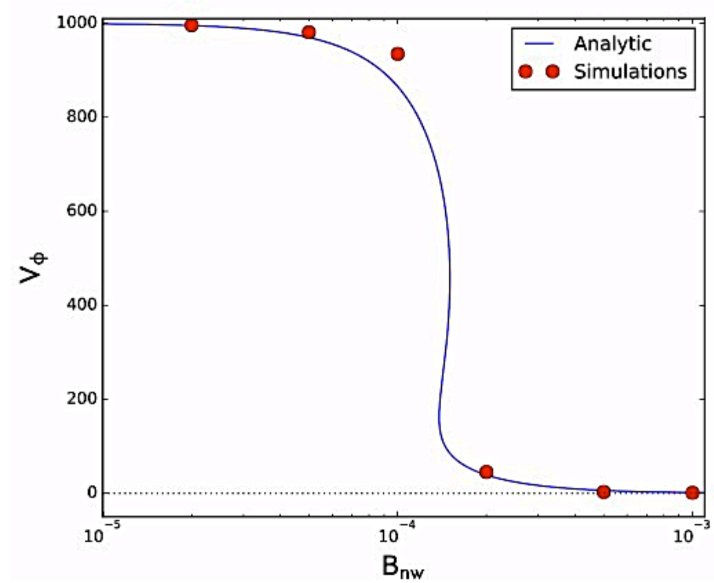

Computed flow at resonance (red) and solution from cubic force-balance (blue) as a function of imposed perturbation.

Case has V_0 = (10/7)V_c ; V_c = 700.

RE study: MST tokamak discharges investigate runaway-electron generation and suppression. [A. DuBois]

- B_ϕ power supply upgrade facilitates MST tokamak operation.
  - $5\times10^{17} \leq n_e \leq 5\times10^{18}$ m^{-3} ; density controlled by gas puffing.
  - $40 \leq I_p \leq 60$ kA; $T_e(0) \cong 120$ eV
  - Arrays of HXR and SXR detectors are used to judge RE presence.
- Factor of 2 difference between n_e to prevent RE & n_e to suppress existing RE:

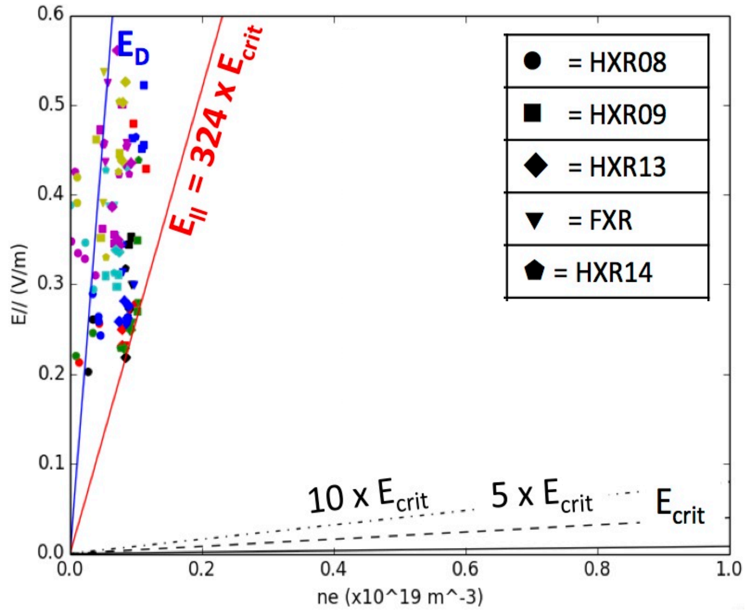

HXR detection showing $E_{||}$ vs. n_e for prevention.

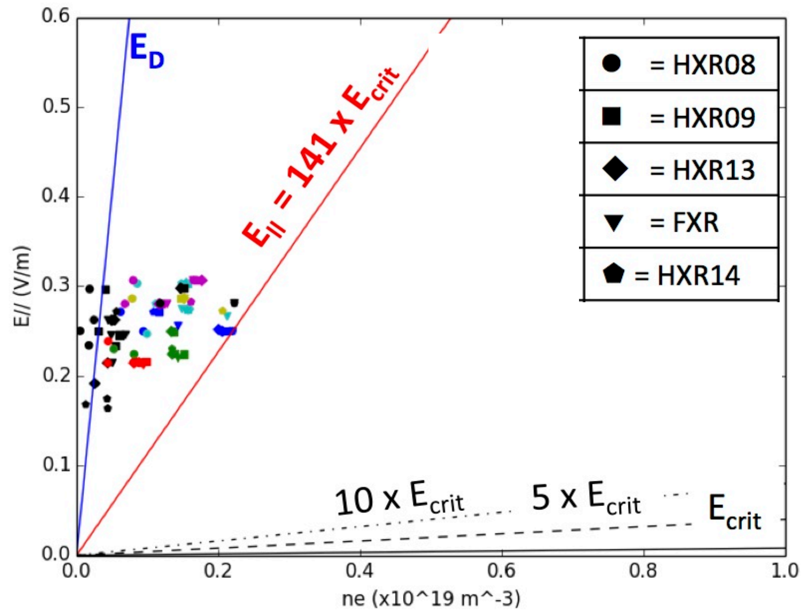

HXR detection showing $E_{||}$ vs. n_e for suppression.

RE confinement is sensitive to the poloidal harmonic content of applied RMPs. [S. Munaretto]

- RMP-drive coils (green) are adjusted to provide a prescribed poloidal harmonic at sensors (white).
  - Applied toroidal spectrum is broad.
  - Present focus is m = 1 and m = 3.
- Discharges have $q(0) < 1$, $q(a)$ = 2.2-2.7.
  - Periodic magnetic fluctuations are observed.

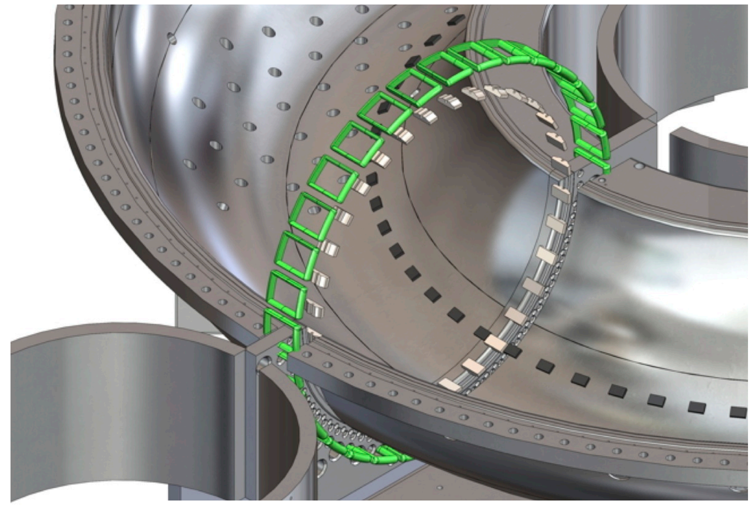

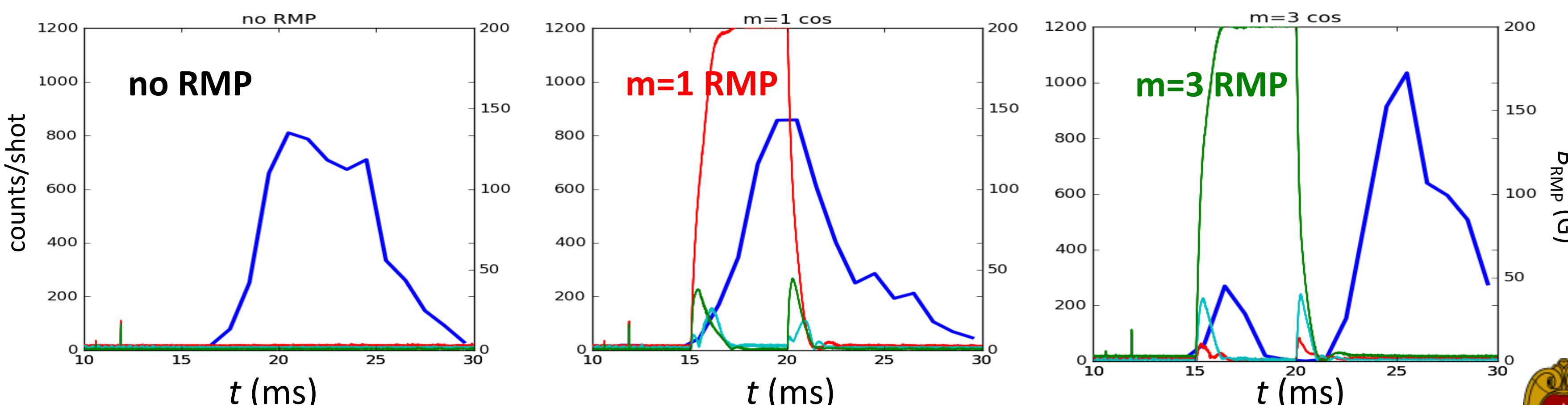

Counts from fast-response poloidal-view HXR detector (5 keV threshold; blue) and applied perturbation (red and green) over time.

The effects of RMP on the magnetic field are being investigated through NIMROD computations. [B. Cornille]

- Linear and nonlinear computations solve resistive-MHD without RE effects.
  - Low-β conditions are modeled with $p = 0$.
  - Effective source drives fitted equilibrium current profile.
  - $S = 10^5$; Pm = 1
- RMP vacuum field is imposed on fitted equilibrium as the initial condition.
  - Toroidal spectrum is limited to ½ toroidal resolution ($0 \leq n \leq 10$).
  - Applied perturbation amplitude is based on MST sensor measurements.

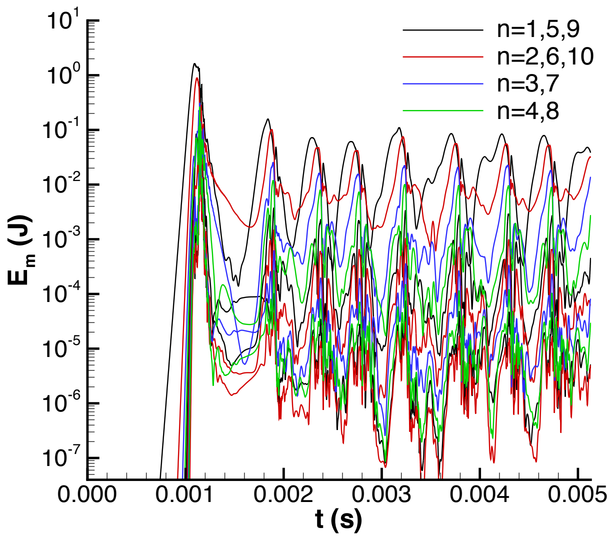

Magnetic fluctuation energy without RMP shows sawtoothing; period in MST is similar.

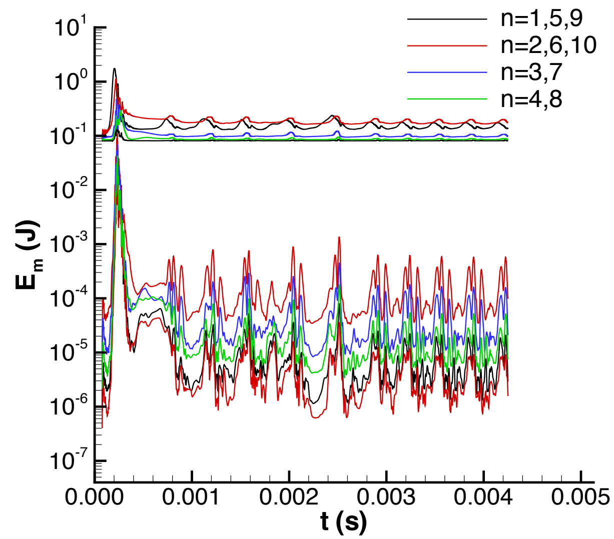

m=3 RMP energy adds to *n*<6 fluctuations; sawtoothing is still evident.

Nonlinear simulation without RMP indicates a large (1,1) inversion layer but no effect on edge.

- Linear computations for the $q(a) = 2.2$ profile show that the (1,1) kink and (2,2) tearing modes are unstable.
- Nonlinearly, the central-q remains near unity after first event (also with RMP).

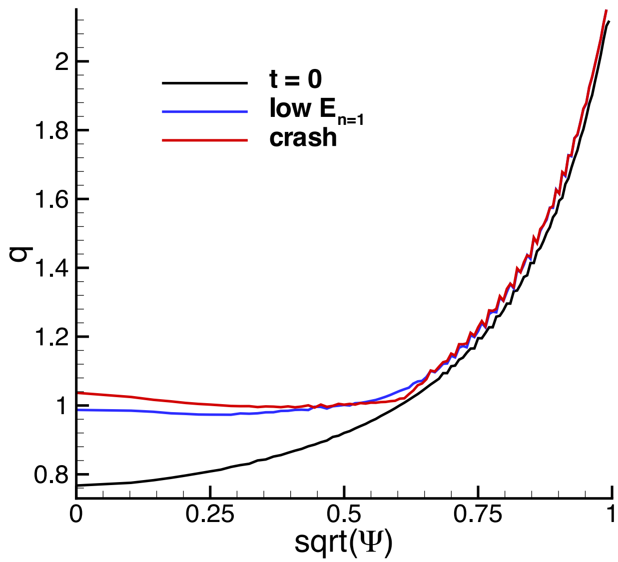

Safety-factor (*q*) at initial state and at different sawtooth phases.

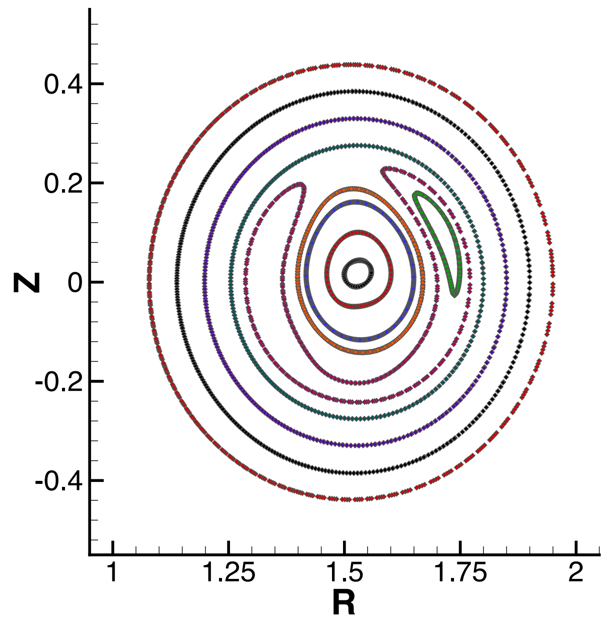

Poincaré plot at low n=1 magnetic energy.

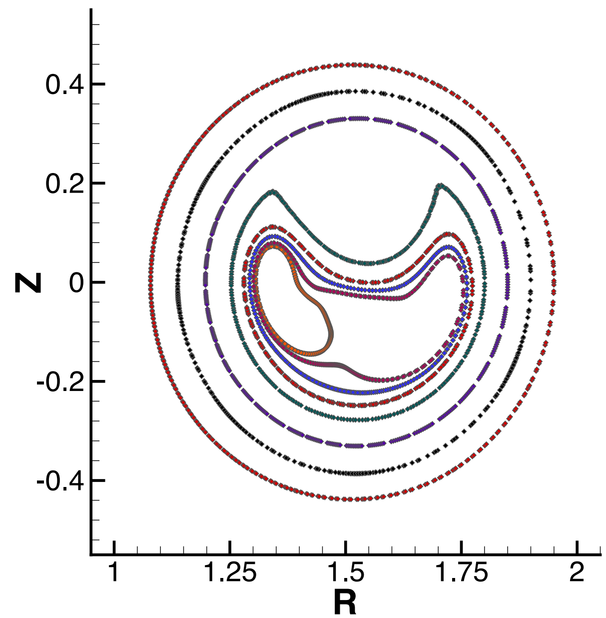

Poincaré plot during crash phase.

Field-line tracing shows chaotic edge region with m = 3 RMP but not with m = 1 RMP, suggestive of RE observations.

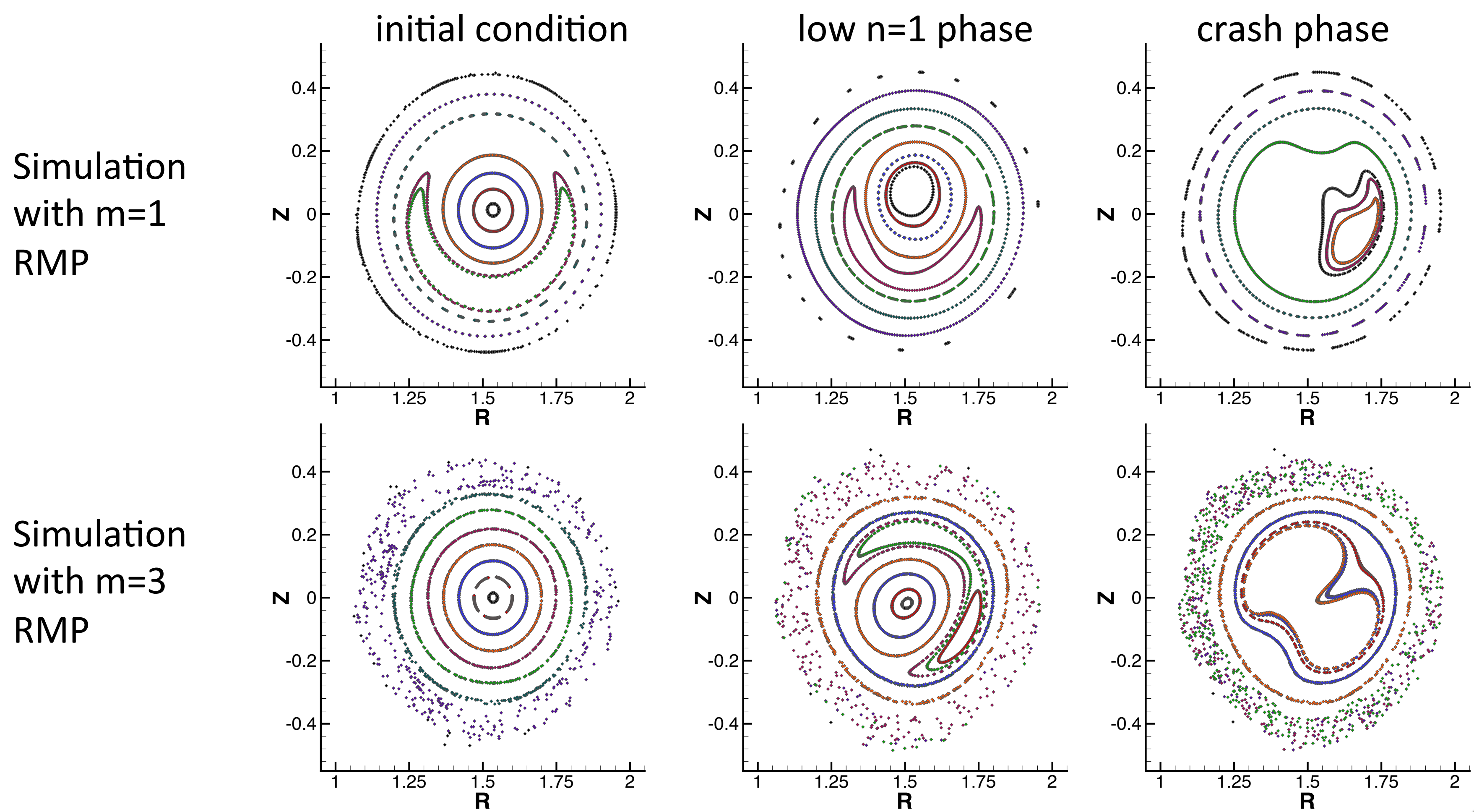

- Vacuum m=1 and m=3 RMPs yield different initial topologies.
- Sawtooth slightly enhances m=3 edge stochasticity. [Results are preliminary!]

Concluding Remarks

- Tracking a plasma surface is improved by least-squares projection.
- Solving ill-conditioned algebraic systems is the primary critical-path issue for robust nonlinear Eulerian simulation of external kink.
- Benchmarking for mode locking is underway.
- The RE study on MST is contributing to ITPA activities.
- We are assimilating experimental and simulation results to understand the effects of RMP on RE confinement in MST.